*J. Fluid Mech.* (2006), *vol.* 550, *pp.* 85–109.  
doi:10.1017/S0022112005008141 Printed in the United Kingdom

# Colliding turbulent plumes

By N. B. KAYE[1] AND P. F. LINDEN[2]

[1]Department of Civil and Environmental Engineering, Imperial College London, Imperial College Road, London, SW7 2AZ, UK.

[2]Department of Mechanical and Aerospace Engineering, University of California, San Diego, 9500 Gilman Drive, La Jolla, CA 92093-0411, USA.

(Received 13 November 2003 and in revised form 8 August 2005)

The collision of axisymmetric turbulent plumes with buoyancy fluxes of opposite sign is examined experimentally. The total buoyancy flux loss of each plume as a result of the collision is measured. The measurements are made using a new experimental technique for measuring the buoyancy flux of a plume based on the ventilation theory of Linden, Lane-Serff & Smeed (*J. Fluid Mech.* vol. 212, 1990, p. 309). The experimental results are presented as functions of the buoyancy flux ratio $\psi$ and the ratio of radial to vertical separation $\sigma$. For axially aligned plumes we find that the lower-buoyancy-flux plume loses all its buoyancy flux when $\psi < 0.3$, and that there is very little buoyancy flux loss for either plume when $\sigma > 0.25$. This plume–plume collision is modelled using a modified set of entrainment equations. The model allows for the exchange of buoyancy and deflection of the plumes as they pass by each other. We present predictions of total buoyancy flux loss as a function of both plume strength and separation. The model predictions are compared to the experimental measurements of buoyancy flux loss, and show good agreement.

## 1. Introduction

Colliding plumes occur when there are two opposing sources of buoyancy in close proximity. For example, an air conditioning vent placed above electronic equipment, such as a computer, will result in plumes that collide. The negatively buoyant plume from the vent will interact with the positively buoyant plume from the computer. For fully developed turbulent plumes, the extent of any interaction will be determined by the geometry of the situation and the relative strengths of the plumes. The stratification produced by plumes of opposite sign has been considered for the case of an enclosed environment (Baines & Turner 1969), and a ventilated environment (Cooper & Linden 1996). However, both analyses assume that the plumes do not interact.

This paper examines the case of two turbulent plumes, with buoyancy fluxes of opposite sign, separated both vertically and horizontally. We begin by reviewing the literature on plume collisions and in § 2 we discuss preliminary observations from visualization experiments and present experimental measurements of buoyancy flux loss. The buoyancy flux measurements are made using a new experimental technique based on the ventilation model of Linden, Lane-Serff & Smeed (1990). Based on experimental observations and measurements, an entrainment model for the exchange of buoyant fluid between the plumes is presented in § 3. The model is used to solve for the total loss of buoyancy flux in each plume as a function of the radial and vertical

separation of the plume sources, and the ratio of the buoyancy fluxes. The model is then compared to our original experimental data. Our conclusions are given in § 4.

Very little work has examined the interaction of colliding plumes, the only relevant paper being Moses, Zocchi & Libchaber (1993). That paper focuses on the starting cap of laminar plumes and the merging of co-flowing laminar plumes, but it also looks at the colliding of approximately equal axisymmetric laminar plumes. Two cases are examined: the axisymmetric problem when the plumes are aligned, and the case of slight misalignment. Turbulent plumes are not discussed.

In the axisymmetric case, the plumes collide and spread out with a sharp interface between the two plumes. No mixing or coalescence was observed, and the disk of plume fluid that resulted from the collision was maintained for some time. All results presented were dimensional, as the effective radius of the Peltier cooler was undetermined. For the case of slight misalignment, the plumes deflect past each other and then rotate around each other. The period of rotation was found to be stable over 10–20 cycles, but varied over longer periods of time. No theory was presented to describe or explain these flows.

Rotation of the type observed by Moses *et al.* (1993) is not restricted to colliding plumes. Konig & Fiedler (1991) observed that a turbulent jet in a counter-flow oscillates around its axis of symmetry. Their paper is mainly concerned with the depth of penetration into the counter-flow, and the mean concentration of a passive scalar in the jet. The authors also observed that the jet oscillates around its axis of symmetry and that the penetration depth fluctuates. The oscillation occurs because the jet has no preferred direction when it is reversed by the counter-flow. The oscillation was also observed when the jet entered the counter-flow at a small angle, but the amplitude of the oscillation decreased as the angle increased. Yoda & Fiedler (1996) suggest that the amplitude of the oscillation is a function of the jet to counter-flow velocity ratio, though this hypothesis is not examined in detail. Similar oscillations are also observed in the height of turbulent fountains (see Turner 1966). Work has also been done on colliding jets by Witze & Dwyer (1976). They showed that two axially aligned turbulent jets with equal momentum flux will collide and spread out in the form of a radial jet.

## 2. Experimental investigation

### 2.1. *Experimental observations*

Preliminary experiments were performed to investigate qualitatively the collision of opposing turbulent plumes. Opposing turbulent plumes were created by adding positively and negatively buoyant fluid, fresh and salt water, respectively, at constant flow rates into a Perspex tank. The tank was initially filled with a saline solution with density at the mean of the two plume source fluids. The axial separation of the plumes varied in the range $0 \leqslant \chi_0/H \leqslant 1$, where $\chi_0$ is the axial separation, and $H$ is the vertical separation of the sources. The buoyancy fluxes of the plumes were approximately equal in magnitude but opposite in sign. Red dye was added to the freshwater plume, and blue dye to the saltwater plume for the purpose of visualization.

Three observations were made. First, when the plumes were almost vertically aligned, they were observed to rotate around each other, as observed by Moses *et al.* (1993) for the slightly misaligned laminar case. The rotation period was not constant, with one plume occasionally dominating the other. After some period of time this flow regime would reverse and the plume that had been dominated would start to deflect and dominate the other. This oscillation was not observed for values of $\chi_0/H$

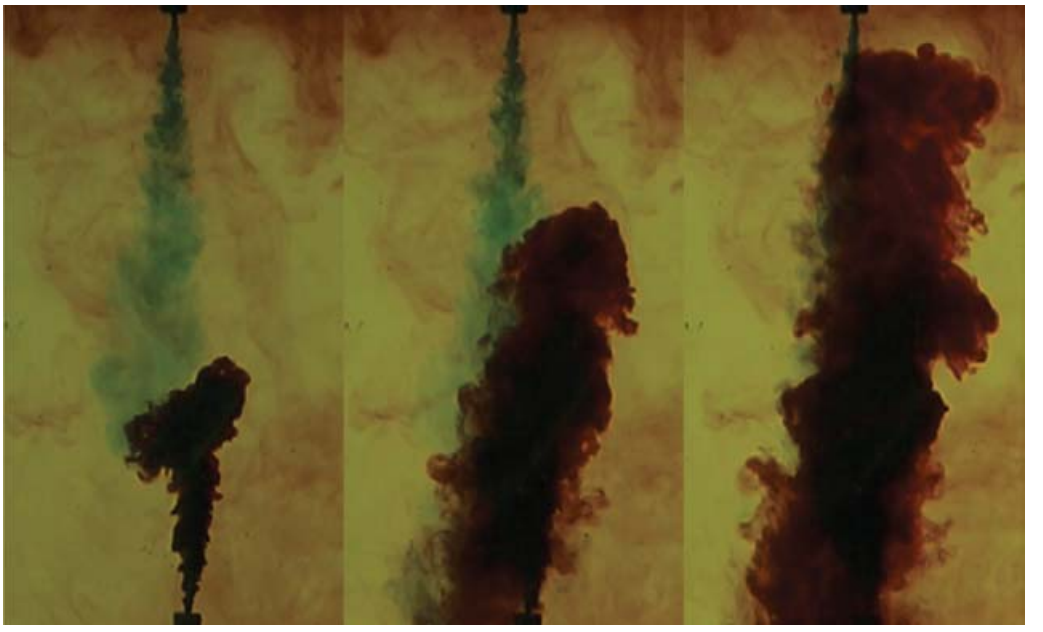

FIGURE 1. A series of images of two aligned opposing turbulent plumes showing the plumes colliding, deflecting past each other and mixing. Note that some of the red dyed lighter plume fluid has mixed with the blue heavy fluid and is flowing downwards. Also note that the ambient remains clear of plume fluid.

greater than about 0.1. It is reasonable to assume that the basic mechanism for this rotation is similar to that of the laminar case, or for a jet in a counter-flow. The plumes deflect past each other but do not have a preferred direction of deflection, so they rotate around their axis of symmetry. A series of images from a visualization experiment is shown in figure 1.

Second, the plumes did not spread out horizontally, as was observed for laminar plumes. Rather they deflected past each other and continued past the source of the opposing plume. This implies that the plumes maintain some form of structural integrity. They do not collide, lose momentum, and mix uniformly. Instead they pass by each other, with mixing occurring along the surface between them. The final observation was that no fluid was ejected from the plumes during the collision. The ambient fluid remained completely clear. This implies that at any height there is only an inflow of fluid into the two plumes. Any fluid of intermediate buoyancy that is created as a result of mixing during the collision is immediately entrained into one of the plumes. After the plumes had passed by the source of the opposing plume they continued to rise (or fall for negatively buoyant plumes) in the form of a turbulent plume. The focus of this experimental investigation is to determine the buoyancy flux of the plumes after they collide.

The final observation, that there is no outflow of neutral fluid into the ambient, is in contrast to both the laminar plume case of Moses *et al.* (1993), and the turbulent jet case of Witze & Dwyer (1976). In both these cases the flows collided and spread out radially. The turbulent plumes do not exhibit this behaviour for two reasons. First, the outflow would be unstable as it would have the heavier fluid from the downward-flowing plume flowing out over the lighter fluid from the upward-flowing plume. Second, as fluid from the two plumes mixes it is re-entrained into one or other

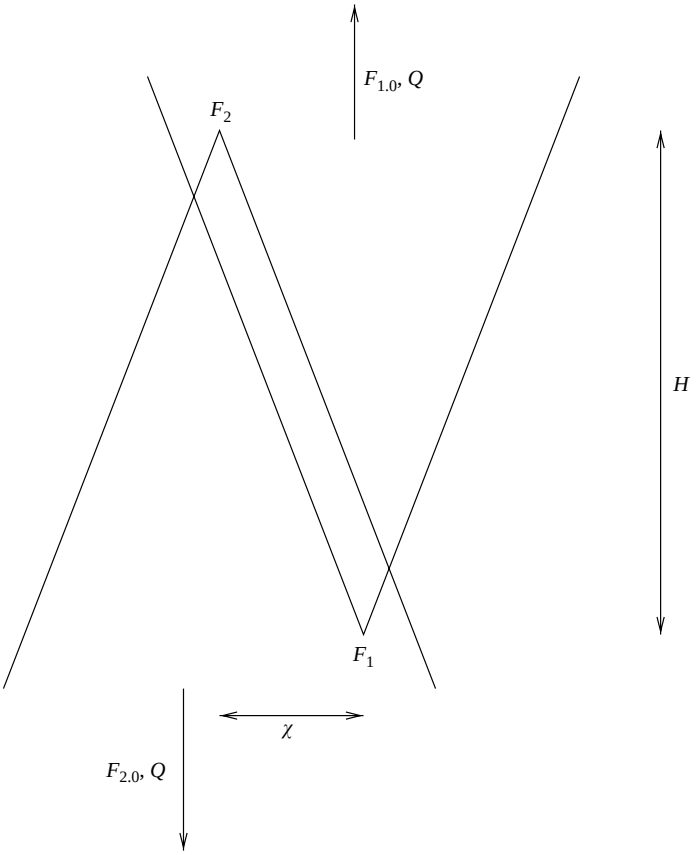


FIGURE 2. Schematic diagram of the parameters governing the collision of opposing turbulent plumes.

of the plumes. The radial outflow observed in the laminar plume case must, therefore, be stabilized by viscosity.

Colliding axisymmetric turbulent plumes can be characterized in terms of four parameters: the buoyancy flux of each plume $F_1$ and $F_2$, the axial separation of the two plumes $\chi_0$, and the vertical separation of the plume sources $H$. This leads to two dimensionless parameters: the buoyancy flux ratio

$$\psi = \frac{|F_2|}{|F_1|} \tag{2.1}$$

and the aspect ratio

$$\sigma = \frac{\chi_0}{H}. \tag{2.2}$$

Note that lengths are scaled on the height not the axial separation to avoid a singularity when there is zero axial separation. We chose the convention that $|F_1| \geqslant |F_2|$, and therefore $0 < \psi \leqslant 1$. Without loss of generality for Boussinesq plumes, the rising plume is taken to have the larger magnitude buoyancy flux. Therefore, $F_1 > 0$, $F_2 < 0$ and $F_1 + F_2 \geqslant 0$. These parameters are shown schematically in figure 2.

The plumes that emerge from the collision region will each have a buoyancy flux denoted as $F_{1.0}$ for the stronger plume and $F_{2.0}$ for the weaker plume. We define the

dimensionless post-collision buoyancy flux of each plume as

$$\eta_1 = \frac{|F_{1.0}|}{|F_1|} \quad \text{and} \quad \eta_2 = \frac{|F_{2.0}|}{|F_1|}. \tag{2.3}$$

By conservation of buoyancy we can write

$$F_{1.0} + F_{2.0} = F_1 + F_2 \tag{2.4}$$

or

$$|F_1 - F_{1.0}| = |F_2 - F_{2.0}|. \tag{2.5}$$

Hence, the magnitude of the buoyancy flux loss in each plume is the same. In dimensionless form (2.5) is

$$1 - \eta_1 = \psi - \eta_2. \tag{2.6}$$

Therefore, for a given value of $\psi$ we only need measure the buoyancy flux of one of the post-collision plumes. We can also use (2.6) to set limits on the value of $\eta_1$. If we assume that there is no mixing at all then each plume will retain its original buoyancy flux and $\eta_1 = 1$ and $\eta_2 = \psi$. If, on the other hand, the plumes mix completely, then the weaker plume will lose all of its buoyancy flux and $\eta_2 = 0$. Therefore, $\eta_1$ will be in the range

$$1 - \psi \leqslant \eta_1 \leqslant 1. \tag{2.7}$$

As all measurements will be focused on the stronger plume we will drop the subscript 1 from $\eta$ when referring to the stronger plume.

### 2.2. *Review of previous techniques*

Various experimental techniques have been used to measure the bulk properties of buoyancy-driven flows. For example, Hacker, Linden & Dalziel (1996) used a light attenuation technique to examine the time-varying buoyancy profile in lock release gravity currents. Morton, Taylor & Turner (1956) measured the rise height of plumes in a stratified ambient and inferred from their measurements the value of the entrainment coefficient.

Light attenuation techniques involve adding a dye to the fluid and measuring how the dye attenuates a light of known intensity. The attenuation is related to the concentration of the dye, which acts as a surrogate for the buoyancy (or passive tracer) that is being measured. In order to use this technique with colliding turbulent plumes, three fluids need to be consistently dyed, the two plumes and the ambient fluid. The only way to do this is to dye the ambient and one plume, while leaving the second plume un-dyed. Assuming that the ambient fluid has a density equal to the average of the densities of the two plume sources, the ambient dye attenuation results in an attenuated light intensity $I$ in the middle of the camera range (say $I = 128$ for a typical 0–255 digital scale), as the dye concentration scales on the density. The source fluids provide intensities of 0 and 255, respectively. Once the plumes mix with the environment their buoyancy is closer to that of the ambient fluid. Typical experiments result in plume buoyancy to source buoyancy ratios of approximately 1/40 over the height of the experiment. This dilution results in intensities approximately in the range of 125 to 131, yielding a total resolution of only 7 points. It is, therefore, only possible to use this technique with plumes of the same sign (Kaye & Linden 2004), because the ambient fluid is not dyed, and the source solution can be dyed such that the full resolution of 256 points can be used once the plume has mixed.

Baines (1983) developed a technique for measuring the volume flow rate in a plume by placing the plume in a tank with a constant ambient flow rate in the same direction

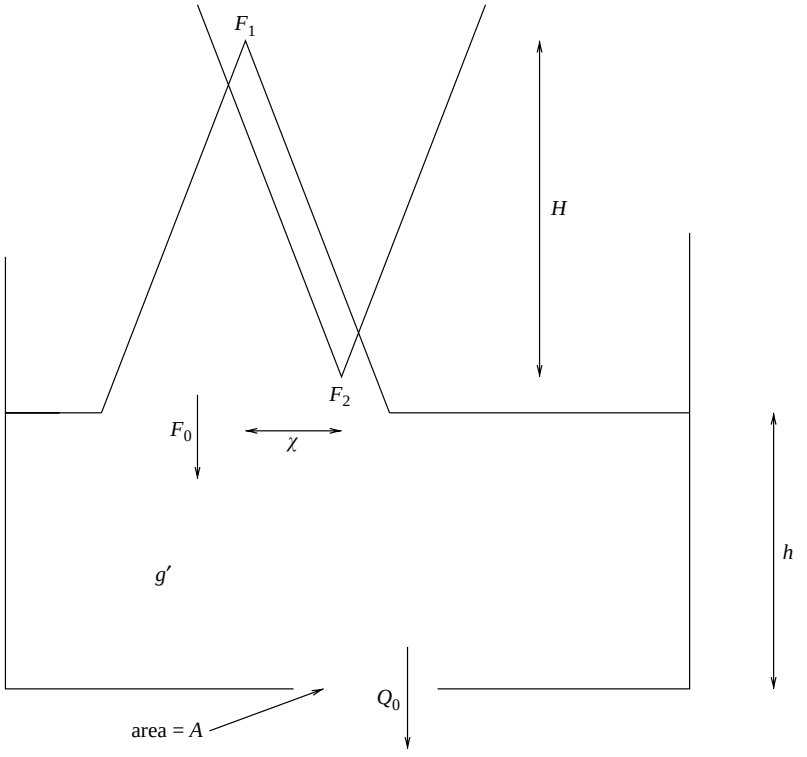


FIGURE 3. Schematic diagram of the experimental set-up for measuring the buoyancy flux loss in colliding plumes. The diagram shows the colliding plumes, the dense layer of thickness $h$ formed below the collision, and the bottom opening and resulting outflow.

as the plume flow. A two-layer stratification develops, with the plume flow rate at the density interface equal to the ambient flow rate. One problem in applying this technique to colliding plumes is that fluid of the ambient density would need to be added in order to hold the density interface in place, which requires pumping a large volume of salt water into the tank at a measured rate. Typically, this would involve volumes of the order of hundreds of litres – mainly a logistical problem. A second problem is that once an interface has been established, any interaction between the colliding plumes below the front (assuming that the falling plume is being measured) would not occur under the same ambient conditions. Note that in this configuration the technique would not measure the flow rate of a single plume, but rather $Q_1(\zeta) - Q_2(\zeta)$.

### 2.3. *Technique developed for measuring buoyancy flux*

To overcome these problems, a new experimental technique was developed to measure the buoyancy flux of a plume. Based on the ventilation model of Linden *et al.* (1990), the technique involves allowing the two plumes to collide and interact, and then catching the falling plume in an open-topped ventilated box. A schematic is shown in figure 3.

Below the interaction area, the falling plume has buoyancy flux $F_{1.0} = \eta_1 F_1$. This plume fills the box to a steady state height $h$, just as in the basic ventilation problem (see Linden *et al.* 1990). The flow rate of the plume through the interface is matched by the draining flow out of the lower opening (denoted by $Q_0$). After an initial

transient period the buoyancy of the layer will be uniform (denoted by $g'_0$), and equal to that of the mean buoyancy of the plume as it enters the lower layer. The buoyancy flux of the plume is then given by

$$F_0 = g'_0 Q_0. \tag{2.8}$$

By sampling the fluid in the dense layer and the ambient, it is possible to establish the buoyancy of the layer $g'_0$. From this it is possible to calculate the flow rate through the box, by using the draining theory of Linden *et al.* (1990), as

$$Q_0 = A^* \sqrt{2 g'_0 h}. \tag{2.9}$$

Provided that the opening area of the inlet is considerably larger than the outlet area $A_0$, then $A^*$ is given by

$$A^* = C_d A_0 \tag{2.10}$$

The buoyancy flux is therefore given by

$$F_0 = \eta F_1 = C_d A_0 \sqrt{2} {g'_0}^{3/2} h^{1/2}. \tag{2.11}$$

As the source buoyancy flux $F_1$ is known, the value of $\eta$ is given by

$$\eta = \frac{C_d A_0 \sqrt{2} {g'_0}^{3/2} h^{1/2}}{F_1}. \tag{2.12}$$

The discharge coefficient $C_d$ for a sharp-edged orifice is typically in the range 0.6 to 0.65 (see Massey 1989, p. 96). To verify this value, experiments were performed using only a single plume of known buoyancy flux (in this case, $\eta = 1$). Averaging over a series of experiments gave a value of $C_d = 0.63 \pm 0.015$, which is within the expected range. A detailed analysis of all errors related to these experiments is given in the Appendix.

Note that the distance between the plume sources is taken as the distance between the nozzle outlets plus the distance to the virtual origin for each plume. The corrections were made using the method presented by Hunt & Kaye (2001) and accounted for about 20 % of the total height (10% at each end).

### 2.4. *Transients and time scales*

When two plumes collide they deflect past each other and oscillate around each other. This oscillation is observed to take a number of forms, with either the two plumes deflecting in opposite directions, or only one plume deflecting and the other tending to dominate the flow. Both situations were observed for equal plumes, though for smaller values of $\psi$ the stronger plume tended to dominate.

As the flow is unsteady, the buoyancy flux draining from the box is not constant. Therefore, it is necessary to take measurements of the buoyancy flux over time and average them. In order to establish the averaging time we consider the draining time, which is the time it takes for a layer of dense fluid to drain out of a ventilated box (Linden *et al.* 1990). This time scale is given by

$$t_e = \frac{A_t}{2 A_o \sqrt{2} C_d} \sqrt{\frac{h}{g'_o}} \tag{2.13}$$

where $A_t$ is the cross-sectional area of the tank. Substituting typical experimental values into (2.13) gives

$$t_e = \frac{513}{2 \times 12.5 \times \sqrt{2} \times 0.63} \sqrt{\frac{10}{0.5}} = 103\,\mathrm{s}, \tag{2.14}$$

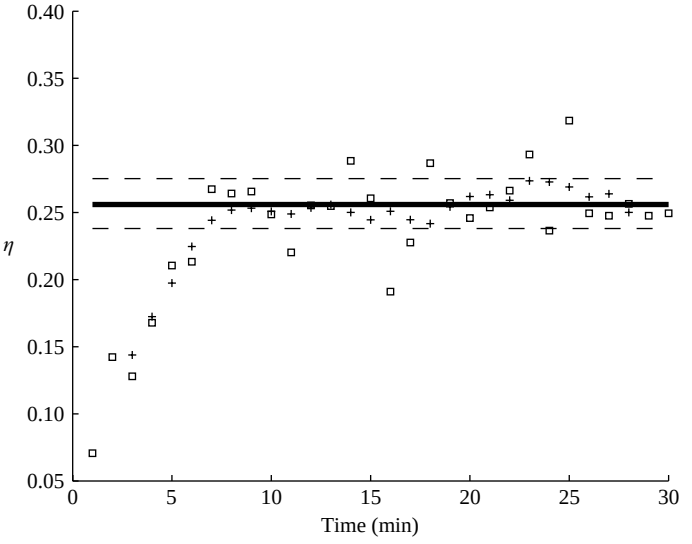


FIGURE 4. Measured values of $\eta$ for $\psi = 0.91$ and $\sigma = 0$. The squares are the instantaneous measured values and the crosses are values averaged over 5 minutes. The solid line is the average over the last 20 minutes and the dashed lines are $\pm 7\,\%$ of that value.

or approximately two minutes. Therefore, variations that occur on this time scale or longer will appear in a time series. Any fluctuations with shorter periods are damped out by the capacity of the box, and so will not be measured.

In order to establish the best averaging procedure, an experiment was run with $\psi = 0.91$ and $\sigma = 0$. Measurements were taken every minute for 30 minutes, from the time the plumes were turned on. The results are plotted in figure 4. The crosses are the instantaneous results, while the squares are a five minute average. The thick line is the average value for the last 20 minutes, and the thin lines are $\pm 7\,\%$ (see (A 3)). The box fills up over a period of $\approx 4t_e$, but significant fluctuations are observed outside the error range predicted earlier. The five minute average ($\approx 3t_e$), however, can be seen to filter out these fluctuations, with all points within the estimated error.

Based on this preliminary experiment, the following procedure was adopted for our experiments. The plumes are turned on, and 17 minutes later (typically $\approx 10t_e$) five measurements are taken at 1 minute intervals, and the time-average determined.

### 2.5. *Results*

Results for the colliding plume experiments are presented for $\psi = 1.0$, 0.8, 0.6, 0.4, and 0.2, with $\sigma$ in the range 0 to 0.3. The results are plotted in figures 5 to 7. The first point to note about the experimental results is that all 34 measured values of $\eta(\psi, \sigma)$ fall within the range required by conservation of buoyancy, see (2.7). This adds to our confidence in only measuring the post-collision buoyancy flux of the stronger plume as $\eta_2$ can be calculated using the measurements for $\eta_1$ and (2.6).

Secondly, with only one exception, there is no measurable buoyancy flux exchange for separations greater than $\sigma \approx 0.25$. For separations less than this ($\sigma < 0.25$) there is a steady decline in $\eta_1$ reaching a minimum when the plumes are axially aligned (note that for $\psi = 0.2$, figure 5(*e*), the four data points with smallest $\sigma$ values are all essentially at the minimum value of $\eta_1 = 1 - \psi = 0.8$). As a zero-order model we assume that for $\sigma = 0.25$ no mixing occurs and $\eta_1$. For aligned plumes we assume the mixing is complete, that is the weaker plume is fully absorbed, and $\eta = 1 - \psi$. We

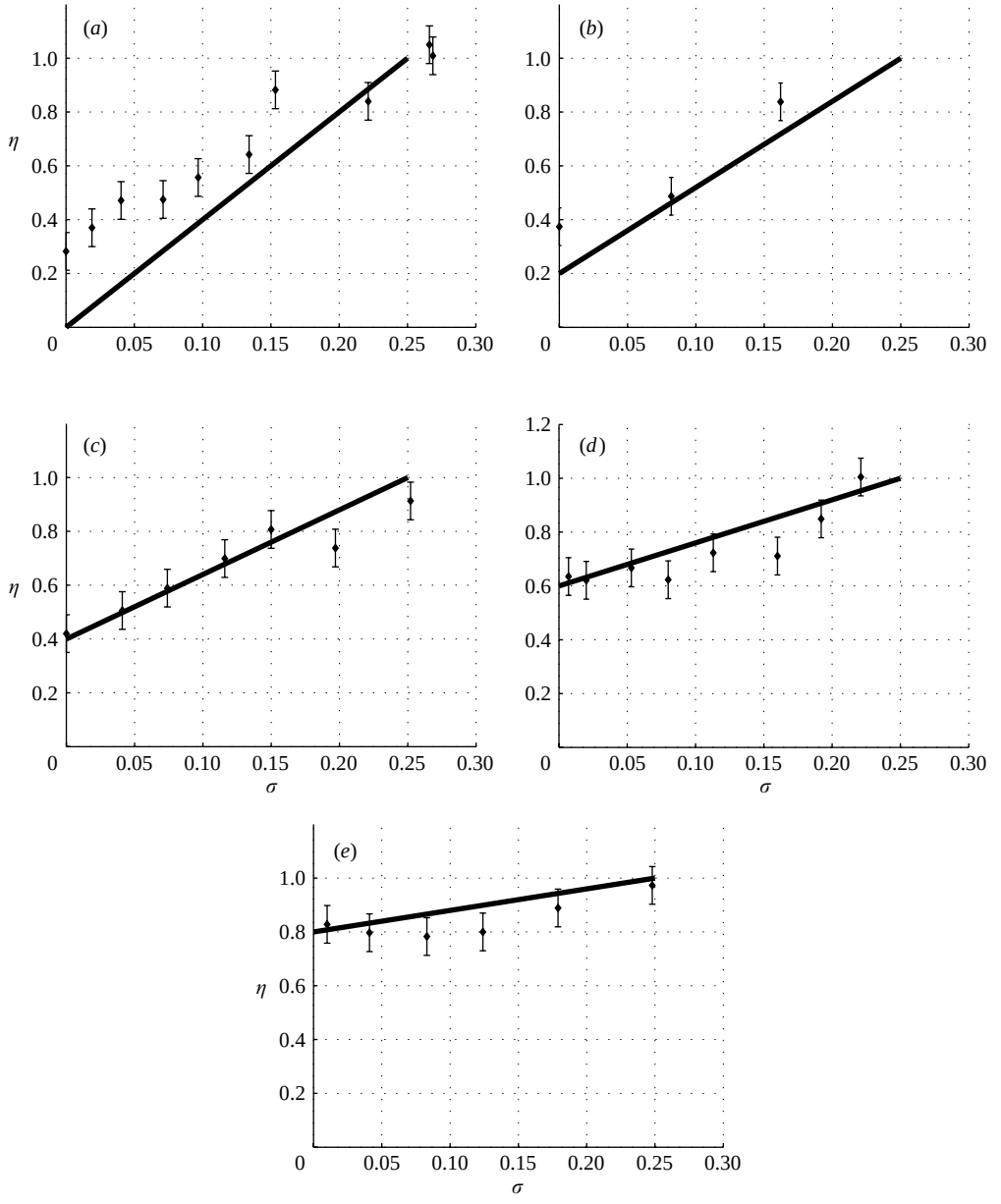


FIGURE 5. Experimental results for $\eta(\sigma)$ with (*a*) $\psi = 1.0$, (*b*) $\psi = 0.8$, (*c*) $\psi = 0.6$, (*d*) $\psi = 0.4$, (*e*) $\psi = 0.2$. The line is given by $\eta = \min(4\psi\sigma + 1 - \psi, 1)$.

therefore plot a line in figure 5, representing a linear interpolation between these two extremes,

$$\eta = 1 - \psi(1 - 4\sigma) \text{ for } 0 < \sigma < 0.25. \tag{2.15}$$

With the exception of $\psi = 0.6$ the majority of points do not lie on the line given by the linear mixing model (2.15). For larger values of $\psi$ there is less mixing and buoyancy flux exchange (larger $\eta$) as the axial separation is reduced. When the plumes

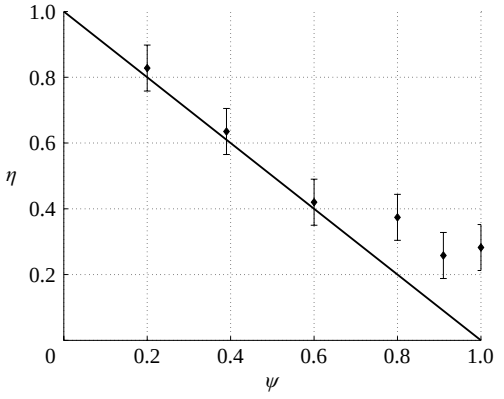


FIGURE 6. Experimental results for $\eta(\psi)$ for $\sigma = 0$. The line $(= 1 - \psi)$ is the minimum possible value while still conserving buoyancy.

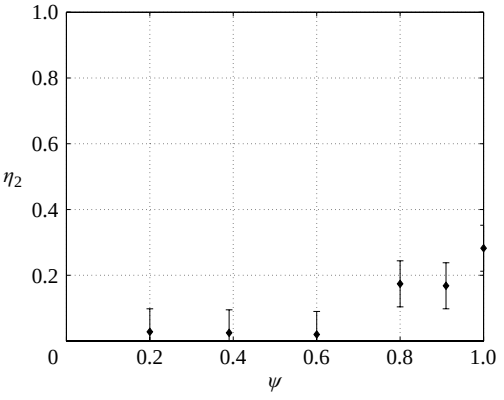


FIGURE 7. Calculated values of $\eta_2(\psi)$ showing the near total absorption of the weaker plume for $\psi < 0.6$.

are aligned ($\sigma = 0$) the total loss in buoyancy flux is less than the minimum value of $\eta_{\min} = 1 - \psi$. For smaller $\psi$ and $\sigma = 0$ the weaker plume is completely absorbed by the stronger plume ($\eta(\psi) \leqslant 0.6 = \eta_{\min}$). As the axial separation is increased the rate of increase of $\eta$ is less than the simple linear model, but increases as $\sigma \to 0.25$. The difference between the measured values of $\eta$ and $\eta_{\min}$ for $\sigma = 0$ and larger values of $\psi$, are shown more clearly in figures 6 and 7.

For the case of aligned plumes ($\sigma = 0$) and small $\psi$ the value of $\eta_1$ is close to the minimum $(= 1 - \psi)$. However, for larger values of $\psi$ this is not the case. This implies that when one plume is significantly stronger than the other it will completely absorb the weaker plume when axially aligned. For more balanced plume strengths there is still substantial mixing, but both plumes 'survive' the collision with reduced buoyancy flux.

Clearly the simple linear model for quantifying the level of mixing between colliding turbulent plumes shows poor agreement with the experimental measurements. We now look for a more sophisticated model to describe the experimental results presented above. The model would ideally capture details that are not included in the linear interpolation. These major discrepancies between the experimental results and the

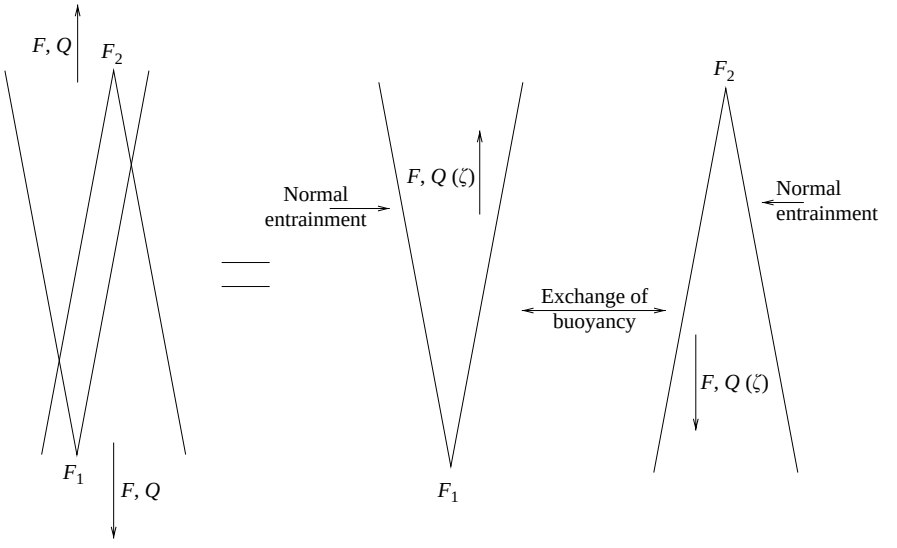


FIGURE 8. Schematic of the entrainment model for colliding plumes. The diagram shows the equivalent system of two plumes that exchange only buoyant fluid.

simple linear model are:

(i) for aligned plumes, $\eta(\psi > 0.6, \sigma = 0) > \eta_{\min}$;

(ii) for $\psi < 0.6$, the rate of increase of $\eta$ with $\sigma$ is less than the linear model.

## 3. Entrainment model for plume collision

We begin our model by recalling that, in the initial visualization experiments reported above, the plumes did not mix and spread out horizontally, but rather passed by each other and continued on as plumes beyond the collision region. It is, therefore, reasonable to assume that the plumes maintain some form of structural integrity throughout the collision. Consequently, we describe the two plumes separately, but with the model for each plume containing mixing terms to account for the interaction between the two plumes. We then write plume conservation equations similar to those of Morton *et al.* (1956) with modifications for the entrainment by each plume from the other. A schematic of this modelling approach is shown in figure 8. This approach is similar to that taken by Bloomfield & Kerr (2000) to model the interaction of the upward and downward flow in turbulent fountains.

The conservation equations written in terms of the plume velocity $w_i$ and radius $b_i$, for a uniform environment and top-hat profiles, are

$$\frac{\mathrm{d}}{\mathrm{d}z}\left(\pi b_i^2 w_i\right) = 2\pi b_i \alpha_t w_i, \tag{3.1}$$

$$\frac{\mathrm{d}}{\mathrm{d}z}\left(\pi b_i^2 w_i^2\right) = \pi b_i^2 g_i', \tag{3.2}$$

$$\frac{\mathrm{d}}{\mathrm{d}z}\left(\pi b_i^2 w_i g_i'\right) = 0. \tag{3.3}$$

The subscript $i = 1, 2$ refers to the plume number, and the subscript $t$ on the entrainment coefficient $\alpha$ means it is the coefficient appropriate for use with top-hat

profiles. Two assumptions are now made regarding the nature and geometry of the plume-to-plume entrainment:

(i) the two plumes interact over the overlapping fraction of their circumferences;

(ii) the fluid exchange between the plumes is the difference between the amount of fluid that each plume would entrain from the other were it part of the ambient.

These two assumptions are discussed in detail below together with two models for buoyancy flux exchange.

### 3.1. *Angle of interaction*

It is assumed that at any height each plume can be taken as circular and that the radius grows linearly with distance from the plume source. This is not strictly correct, as the plumes will not be self-similar in the interaction region as each will be deformed by the presence of the other. Nevertheless, the circle assumption provides a starting point for scaling the extent of the plume interaction. The assumption that the plumes can be modelled as overlapping circular cones means that at any height a certain fraction of the circumference of each will overlap the other plume. The angles of the overlap are denoted by $2\theta_i$ and vary with height.

The choice of radius $r_i(z)$ is essentially arbitrary, but needs careful consideration, as it is assumed that for separations greater than the sum of the two plume radii no interaction will occur (note that each plume radius grows linearly with height in opposite directions, therefore the sum of their radii is constant). We could choose a radius such that no interaction occurs for $\sigma > 0.25$ based on our earlier experimental results. However, there are insufficient data to establish accurately this value from our experiments. The model we present here also accounts for the drawing together of the plumes due to the entrainment velocity in a manner similar to that for co-flowing plumes Kaye & Linden (2004). Therefore a smaller starting radius is required. The obvious choices for the radius are the top-hat profile radius, the radius of the equivalent Gaussian profile ($r_i = \sqrt{2} r_g$), and a radius given by the distance at which the mean buoyancy is a certain fraction of the centreline value (say 5 %). Interaction will still occur when the plumes are at a separation slightly greater than the Gaussian radius as the turbulent edge of the plume is further away from the axis. A greater length is required, and for this reason the third choice, the 5 % radius, is used as a first approximation. The radius of each plume is then given by

$$\xi_1 = \frac{6\alpha_g \zeta}{5}\sqrt{|\ln(0.05)|}, \quad \xi_2 = \frac{6\alpha_g (1-\zeta)}{5}\sqrt{|\ln(0.05)|}, \tag{3.4}$$

where $\xi_i = r_i/H$ and $\alpha_g = \alpha_t/\sqrt{2}$. It is important to note that the radius is independent of $\psi$ and that for separations greater than the maximum radius ($\sigma_0 > (6\alpha_g/5)\sqrt{|\ln(0.05)|} = 0.19$), no interaction will occur in this model (as $\theta_1 = \theta_2 = 0$). The angles $\theta_1$ and $\theta_2$ are given by

$$\cos\theta_1 = \frac{\sigma_0^2 + \xi_1^2 - \xi_2^2}{2\sigma_0\xi_1}, \quad \cos\theta_2 = \frac{\sigma_0^2 + \xi_2^2 - \xi_1^2}{2\sigma_0\xi_2}. \tag{3.5}$$

It is assumed that when one plume completely surrounds the other, the angle for the larger radius plume is 0 and the other angle is $\pi$.

A plot of $\theta_1$ as a function of height is shown in figure 9, for various values of $\sigma$. For clarity, height is plotted vertically. The plot indicates that, for larger values of $\sigma$, the height over which there is a large angle of interaction is smaller (for example, for $\sigma = 0.18$ $\theta_1 < 0.8$ for $\zeta > 0.1$). For smaller separations, the height at which $\theta_1 < 0.8$ increases ($\zeta > 0.5$ for $\sigma = 0.12$ and $\zeta > 0.6$ for $\sigma = 0.06$). For plumes with no axial separation ($\sigma = 0$) $\theta_1 = \pi$ for $\zeta < 0.5$ and $\theta_1 = 0$ for $\zeta > 0.5$. This implies that the rising

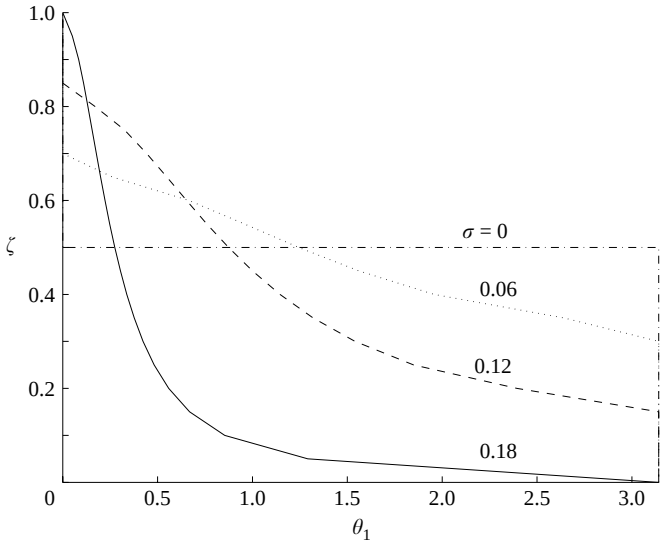


FIGURE 9. Plot of $\theta_1$ as a function of $\zeta$ for $\sigma = 0$, 0.06, 0.12 and 0.18.

plume is completely surrounded by the falling plume until the point halfway between the sources, and then the rising plume surrounds the falling plume above that height.

### 3.2. *Exchange of volume flux*

As discussed earlier, the main consequence of the collision of two plumes is a reduction in the buoyancy flux of each plume. In order for this to occur, the plumes must exchange fluid. To calculate the amount of fluid drawn into each plume at any height we assume that each plume regards the other as part of the ambient fluid. We then calculate the rate of entrainment into each plume based on the entrainment velocity, plume radius and the angle of overlap. The amount of fluid entrained into the 'dominant' plume is taken to be the difference $\Delta$ between these two calculated values. The 'dominated' plume loses the same volume of fluid. The entrainment term on the right-hand side of (3.1) will contain the regular entrainment term for a sector of angle $2(\pi - \theta_i)$ plus the difference between the calculated entrainment rates $\Delta$. The difference between the entrainment rates is given by

$$\Delta = 2\alpha_t(\theta_i b_i w_i - \theta_j b_j w_j). \tag{3.6}$$

Equation (3.1) therefore becomes

$$\frac{\mathrm{d}}{\mathrm{d}z}\left(\pi b_i^2 w_i\right) = 2\alpha_t(\pi b_i w_i - \theta_j b_j w_j), \tag{3.7}$$

where $j \neq i$. The values of $w_i$ and $w_j$ are taken as the magnitudes of the plume velocities, and are always positive. Note that (3.7) is equivalent to (3.1) with an additional term for the fluid removed from the plume due to entrainment by the other.

### 3.3. *Exchange of buoyancy flux*

Having established an estimate of the volume flux exchanged at any height, we need to examine possible models for the exchange of buoyancy flux. There are two models to consider. One possibility is that we could assume that entrainment is a two-way process and that, at each height, each plume entrains fluid from the other

and buoyancy exchange is in both directions. In that case the appropriate expression for the buoyancy flux exchange is

$$\frac{\mathrm{d}}{\mathrm{d}z}\left(\pi b_i^2 w_i g_i'\right) = 2\alpha_t(\theta_i b_i w_i g_j' - \theta_j b_j w_j g_i'). \tag{3.8}$$

Alternatively, the entrainment could be regarded as an essentially one-way process at any given height. That is, at any given height fluid exchange between the plumes occurs in only one direction. The buoyancy transfer would therefore be the net fluid transfer rate multiplied by the mean buoyancy of the plume that is net losing fluid. Hence, if $\Delta > 0$, the plume $i$ is gaining fluid (3.6) and the buoyancy exchange is given by $\Delta g_j'$. On the other hand if $\Delta < 0$, the buoyancy exchange is given by $\Delta g_i'$. In this case the net buoyancy exchange is given by

$$\Delta g_k' \begin{cases} k = i, & \Delta < 0 \\ k = j, & \Delta > 0. \end{cases} \tag{3.9}$$

The equivalent expression to (3.8) for this entrainment model is

$$\frac{\mathrm{d}}{\mathrm{d}z}\left(\pi b_i^2 w_i g_i'\right) = 2\alpha_t(\pi b_i w_i - \theta_j b_j w_j) g_k'. \tag{3.10}$$

We will refer to these models as (A) for the bidirectional exchange model and (B) for the unidirectional exchange model. Note that the rate of exchange of volume flux at any height is the same for both models.

### 3.4. *Other potential changes to the plume equations*

The above modifications to the plume entrainment equations account for the exchange of buoyancy between the two plumes. Other changes could also be made. The model ignores any momentum loss due to the collision. This is a reasonable omission based on the observation made earlier that the plumes tend to pass around each other rather than block each other. This observation does not, however, mean that the plumes will not exchange momentum due to entrainment. It could also be argued that each plume will be relatively more buoyant when interacting with the opposing plume as the net buoyancy difference between the plume and its surroundings is greater due to the presence of the opposing plume. We could, therefore, add a term for the exchange of momentum $\sim(-\Delta w_k)$ to (3.2) and a second term to (3.2) to account for the difference in perceived ambient buoyancy $\sim(+\theta_i b_i^2 g_j')$. We have chosen not to add these terms for two reasons. First, the terms are of opposite sign and will tend to cancel each other out. More importantly, however, for a first-order correction the terms of greatest significance will be those that alter the plume driving forces, that is, their buoyancy fluxes. Hence, we focus on the exchange of buoyancy and ignore other possible corrections.

### 3.5. *Full non-dimensional equations*

These equations can be rewritten in terms of the bulk properties of the plume to give

$$\frac{\mathrm{d}Q_i}{\mathrm{d}z} = \alpha_t\left(2M_i^{1/2} - \frac{2\theta_j}{\pi}M_j^{1/2}\right), \tag{3.11}$$

$$\frac{\mathrm{d}M_i}{\mathrm{d}z} = \frac{F_i Q_i}{M_i} \tag{3.12}$$

and

$$\frac{\mathrm{d}F_i}{\mathrm{d}z} = \frac{2\alpha_t}{\pi}\left(\theta_i M_i^{1/2}\frac{F_j}{Q_j} - \theta_j M_j^{1/2}\frac{F_i}{Q_i}\right) \tag{3.13a}$$

or

$$\frac{\mathrm{d}F_i}{\mathrm{d}z} = \frac{2\alpha_t}{\pi}\left(\theta_i M_i^{1/2} - \theta_j M_j^{1/2}\right)\frac{F_k}{Q_k}, \tag{3.13b}$$

where $F = b^2 w g'$, $M = b^2 w^2$, $Q = b^2 w$, and the subscript $k$ is the same as used in (3.9). For the purpose of solving these equations it is convenient to non-dimensionalize them in terms of the fluxes of a pure plume. This results in the dimensionless variables $q_i$, $m_i$ and $f_i$ defined by

$$Q_i = q_i \left(\frac{5F_1}{8\alpha_t}\right)^{1/3}\left(\frac{6\alpha_t H}{5}\right)^{5/3}, \tag{3.14}$$

$$M_i = m_i \left(\frac{5F_1}{8\alpha_t}\right)^{2/3}\left(\frac{6\alpha_t H}{5}\right)^{4/3}, \tag{3.15}$$

$$F_i = f_i F_1. \tag{3.16}$$

Then equations (3.12)–(3.14) become

$$\frac{\mathrm{d}q_i}{\mathrm{d}\zeta} = \frac{5}{6}\left(2m_i^{1/2} - \frac{2\theta_j}{\pi}m_j^{1/2}\right), \tag{3.17}$$

$$\frac{\mathrm{d}m_i}{\mathrm{d}\zeta} = \frac{4}{3}\frac{f_i q_i}{m_i} \tag{3.18}$$

and

$$\frac{\mathrm{d}f_i}{\mathrm{d}\zeta} = \frac{5}{3\pi}\left(\theta_i m_i^{1/2}\frac{f_j}{q_j} - \theta_j m_j^{1/2}\frac{f_i}{q_i}\right) \tag{3.19a}$$

or

$$\frac{\mathrm{d}f_i}{\mathrm{d}\zeta} = \frac{5}{3\pi}\left(\theta_i m_i^{1/2} - \theta_j m_j^{1/2}\right)\frac{f_k}{q_k}. \tag{3.19b}$$

The boundary conditions are assumed to be those for pure plumes at their asymptotic (virtual) origin and are given by

$$q_1 = 0,\ m_1 = 0,\ \text{and}\ f_1 = 1\ \text{at}\ \zeta = 0, \tag{3.20}$$

$$q_2 = 0,\ m_2 = 0,\ \text{and}\ f_2 = \psi\ \text{at}\ \zeta = 1. \tag{3.21}$$

Equations (3.17)–(3.19), subject to (3.20) and (3.21), were solved numerically. The technique involved solving the equations for plume 1 as if plume 2 were a pure plume with no interaction. The results for plume 1 were then used to calculate the right-hand side of the equations for plume 2. This process was repeated, alternating between plumes, until the solutions for each plume converged. The convergence criterion required the difference between iterations to be less than 0.001 for all three fluxes.

### 3.6. *Comparison of model solutions*

The model developed above can be used to solve for the fluxes of buoyancy, momentum and volume for each plume at any height. However, this model seeks to establish the net loss of buoyancy flux as a result of a collision between plumes. Therefore, we do not report momentum and volume flux predictions and instead focus on buoyancy fluxes.

In § 2 we presented measurements of the total loss of buoyancy flux after a collision, but did not consider the loss as a function of height. The loss in buoyancy flux can

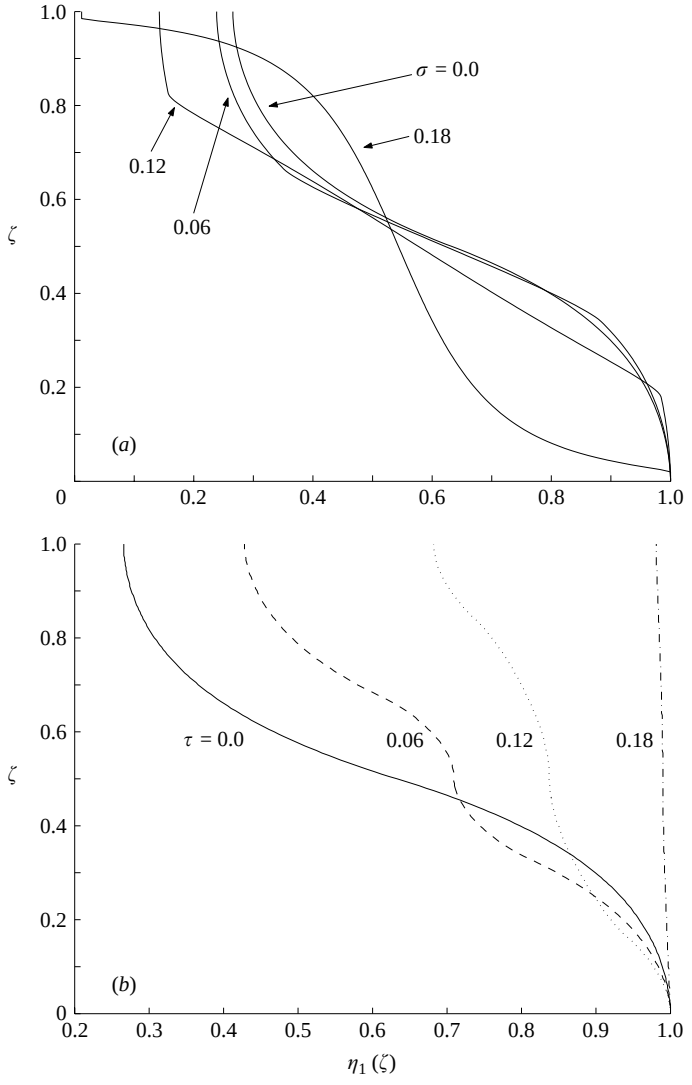


FIGURE 10. Plot of the buoyancy flux loss $\eta$ as a function of distance from the plume source $\zeta$ for ($a$) the bidirectional buoyancy exchange model (A) and ($b$) the unidirectional buoyancy exchange model (B), and aspect ratios of $\sigma = 0$, 0.06, 0.12 and 0.18.

also be described by the parameter $\eta_i$ defined here as

$$\eta_i(\zeta, \sigma) = \frac{F_i(\zeta, \sigma)}{F_1}. \tag{3.22}$$

Plots of $\eta_1(\zeta, \sigma)$ for $\psi = 1.0$ are shown in figure 10($a$) for model (A) and figure 10($b$) for model (B). The plots show how the buoyancy flux decreases with height for various values of the aspect ratio $\sigma$ for each of the two proposed entrainment models.

For the case of the bidirectional entrainment model (A), shown in figure 10($a$), we note that the total buoyancy loss increases with separation. This is more clearly seen in figure 11 which shows a plot of $\eta(\sigma)$ with $\psi = 1$ for both buoyancy exchange

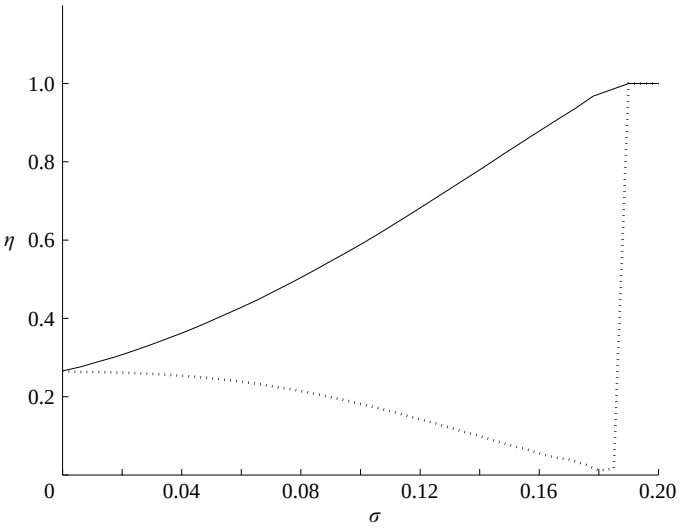


FIGURE 11. Plot of $\eta(\sigma)$ for $\psi = 1$. The solid line represents the unidirectional buoyancy exchange model (B) while the dotted line represents model (A).

models. For closely aligned plumes the bulk of the buoyancy flux loss is in the centre of the flow with only minimal losses near each plume source. However, for larger separations the bidirectional model shows significant buoyancy flux exchange near each plume source. This results from the fact that near the source the plume buoyancy is very large (in fact it is singular at the origin) so, if the opposing plume extracts even a small amount of fluid from the plume near the source, it will result in a significant exchange of buoyancy flux. This does not occur for more closely aligned plumes as the opposing plume completely surrounds the plume near the source and, therefore, has zero angle of interaction (while the other plume has an angle of interaction of $2\pi$).

For the unidirectional model (B) this large-scale near-source buoyancy flux exchange does not occur as the net fluid transfer is into the plume that is nearest its origin. When the plumes are aligned vertically ($\sigma = 0$) most of the mixing occurs between $0.3 < \zeta < 0.7$ where $\eta$ drops from around 0.9 to 0.3, implying a loss of 60 % of the initial buoyancy flux of the plume. This behaviour is the same as for model (A) as the angle of interaction assumption of § 3.1 implies that, for the first half of its travel from the source, the plume can only gain fluid (as it is surrounded by the other plume), whereas for the second half it can only lose fluid since it completely surrounds the other plume. For larger separations, this concentration of mixing in the middle third of the flow is less pronounced.

We now compare models (A) and (B) for $\psi = 1$ as a function of the plume separation. A plot of the net buoyancy flux parameter $\eta(\sigma)$ is given in figure 11, which shows that model (A) predicts an increase in mixing as the plume separation increases until the plumes are no longer touching, at which point there is no buoyancy flux loss. Model (B), on the other hand, predicts a decrease in buoyancy flux exchange as the separation increases. Although we have no direct measurements of how buoyancy exchange occurs at any given height, figure 11 suggests that the unidirectional buoyancy exchange model more accurately tracks the experimental results presented in § 2. For that reason we will continue to develop our model using (3.19*b*).

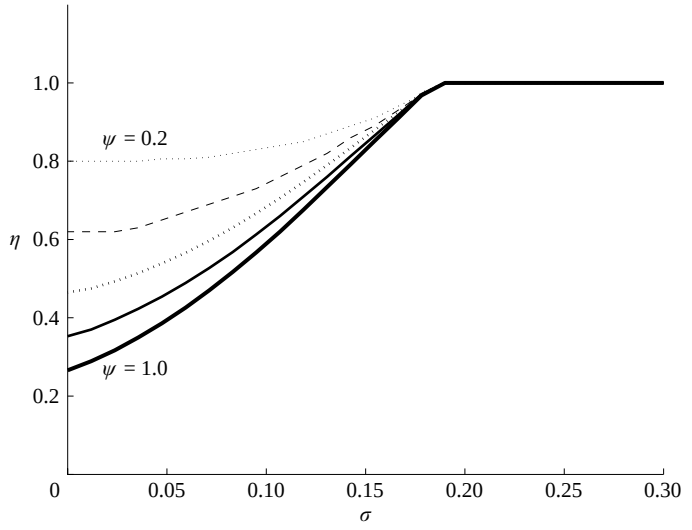


FIGURE 12. $\eta$ as a function of $\sigma$ for $\psi = 1.0$, 0.8, 0.6, 0.4 and 0.2. The lowest line is for $\psi = 1.0$ and the highest is for $\psi = 0.2$.

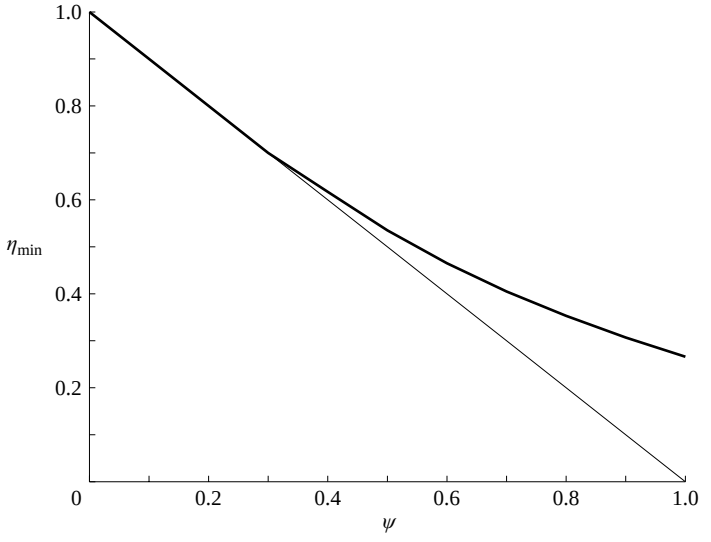


FIGURE 13. $\eta_{\min}$ as a function of $\psi$. The thin straight line ($= 1-\psi$) shows the lowest value $\eta_{\min}$ that can be achieved while conserving buoyancy, and the thick line shows the value predicted by the colliding plumes entrainment model.

### 3.7. *Details of entrainment model (B) solution*

A plot of $\eta_1(\sigma, \psi)$ for model (B) is shown in figure 12. A number of points are worth noting. First, the minimum value of $\eta$ (that is, the maximum loss in buoyancy flux) occurs when the plumes are aligned vertically, with $\eta$ increasing with separation. Second, the value of $\eta_{\min}(\psi = 1)$ is not always zero; even when the plumes are aligned, they do not cancel each other out. In fact, only for $\psi < 0.3$ is the weaker plume completely entrained into the stronger plume. This result is shown more clearly in figure 13, which plots the predicted value of $\eta_1$ for $\sigma = 0$. This plot also shows

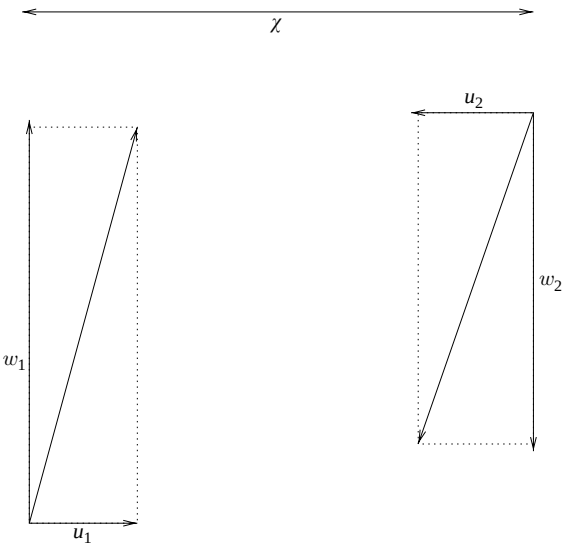


FIGURE 14. Velocity vector diagram for unequal colliding plumes.

the minimum possible value of $\eta_1 = 1 - \psi$ that would occur if the weaker plume were completely absorbed. The predicted value of $\eta_1$ is higher than $\eta_{\min}$ for $\psi > 0.3$, and equal to $\eta_{\min}$ for $\psi < 0.3$.

The model presented above assumes that the plumes entrain from each other, but that each is otherwise unaffected by the presence of the other. However, two plumes in close proximity to each other will tend to draw together due to the ambient velocity field caused by entrainment into the plumes (Kaye & Linden 2004). We now apply a first-order correction to our model to account for this tendency to draw together.

### 3.8. *Plume deflection*

Based on experimental results (for example, Rouse, Yih & Humphreys 1952) it is reasonable to approximate the ambient velocity field outside a single plume, created by entrainment into a plume, as a horizontal flow. The radial velocity into the plume is therefore given by $u(r) = -\alpha w r$ where $w$ is the vertical velocity in the plume, $\alpha$ the entrainment coefficient and $r$ the radial distance from the plume centreline. Gaskin, Papps & Wood (1995) showed experimentally that, for ambient velocities of the same order as the entrainment velocity, the two velocity fields can be added, and this result will be used below. Furthermore, the entrainment flow into each plume is irrotational and governed by Laplace's equation. The linearity of this equation justifies the addition of the two fields. It is, therefore, reasonable to assume that each plume is passively advected by the entrainment field of the other. The velocity vector diagram showing how each plume is deflected by the presence of the other is shown in figure 14.

The values for the velocities can be calculated from the solution to (3.17), (3.18) and (3.19), but as a first-order approximation it is assumed that the pure-plume velocities can be used. The values of $w_1$, $w_2$, $u_1$, and $u_2$ are given by

$$w_1 = c^* F_1^{1/3} z^{-1/3}, \quad w_2 = c^* F_1^{1/3} \psi^{1/3} (H - z)^{-1/3}, \tag{3.23}$$

$$u_1 = c^* F_1^{1/3} \psi^{1/3} (H - z)^{-1/3} \alpha \frac{b_2}{\chi}, \quad u_2 = c^* F_1^{1/3} z^{-1/3} \alpha \frac{b_1}{\chi}. \tag{3.24}$$

Treating each plume separately leads to

$$\frac{\mathrm{d}\chi_1}{\mathrm{d}z} = -\frac{u_1}{w_1}, \quad \frac{\mathrm{d}\chi_2}{\mathrm{d}z} = -\frac{u_2}{w_2}. \tag{3.25}$$

Taking the plumes as conical, with radii given by

$$b_1 = \frac{6\alpha z}{5}, \quad b_2 = \frac{6\alpha(H-z)}{5} \tag{3.26}$$

equation (3.24) becomes

$$\frac{\mathrm{d}\chi_1}{\mathrm{d}z} = \frac{6\alpha_t^2}{5\chi_1}\psi^{1/3}(H-z)^{2/3}z^{1/3}, \quad \frac{\mathrm{d}\chi_2}{\mathrm{d}z} = \frac{6\alpha_t^2}{5\chi_2}\psi^{-1/3}(H-z)^{1/3}z^{2/3}. \tag{3.27}$$

Dividing both sides by $H^2$ and integrating leads to

$$\tfrac{1}{2}\left(\sigma_1^2 - \sigma_0^2\right) = -\frac{6\alpha^2}{5}\psi^{1/3}\int_0^{\zeta}(1-\zeta^*)^{2/3}\zeta^{*1/3}\,\mathrm{d}\zeta^*, \tag{3.28}$$

$$\tfrac{1}{2}\left(\sigma_2^2 - \sigma_0^2\right) = -\frac{6\alpha^2}{5}\psi^{-1/3}\int_0^{\zeta}(1-\zeta^*)^{1/3}\zeta^{*2/3}\,\mathrm{d}\zeta^*. \tag{3.29}$$

Approximating $(1-\zeta)^{2/3}$ by

$$(1-\zeta)^{2/3} \approx 1 - \frac{2}{3}\zeta - \frac{1}{9}\zeta^2 - \frac{4}{81}\zeta^3 - \frac{7}{243}\zeta^4 \ldots \tag{3.30}$$

means (3.27) that can be evaluated as

$$\sigma_1 = \sqrt{\sigma_0^2 - \psi^{1/3}\frac{12\alpha_t^2}{5}\sum(\zeta)} \tag{3.31}$$

with

$$\sum(\zeta) = \frac{4}{3}\zeta^{4/3} - \frac{2}{7}\zeta^{7/3} - \frac{1}{30}\zeta^{10/3} - \frac{4}{351}\zeta^{13/3}. \tag{3.32}$$

The deflection of plume 2 is given by

$$\sigma_2 = \sqrt{\sigma_0^2 - \psi^{-1/3}\frac{12\alpha_t^2}{5}\sum(1-\zeta)}. \tag{3.33}$$

The total reduction in axial separation of the two plumes is therefore given by

$$\sigma = \sigma_1 + \sigma_2 - \sigma_0. \tag{3.34}$$

The average separation $\overline{\sigma}$ over the height was then calculated and a coordinate transformation function $\overline{\sigma}(\sigma_0)$ evaluated. A plot of this transformation is shown in figure 15. Two points are worth noting. First, for initial separations of $\sigma_0 < 0.08$ the mean separation is zero. Second, the transformation is insensitive to variations in $\psi$ over the range $0.2 < \psi < 1.0$, because the mean velocity of the plume is only a weak function of the buoyancy flux.

### 3.9. *Corrected solution*

A quadratic curve was fitted to the data plotted in figure 15 ($\sigma_0 = 0.08 + 0.5\overline{\sigma} + 1.02\overline{\sigma}^2$), which allowed a correction to figure 12 for the drawing together of the plumes. The corrected plot of $\eta(\sigma_0, \psi)$ is shown in figure 16.

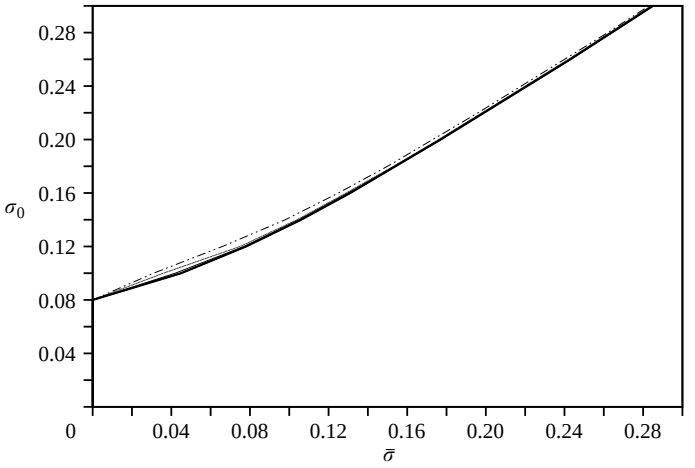


FIGURE 15. Plot of the coordinate transformation $\bar{\sigma}(\sigma)$ where $\sigma$ is plotted vertically. The function is shown for values of $\psi = 1.0$, 0.8, 0.6, 0.4, and 0.2. The thickest line is for $\psi = 1.0$ and the dot-dashed line is for $\psi = 0.2$. Note that most lines overlap and are not clearly distinguishable.

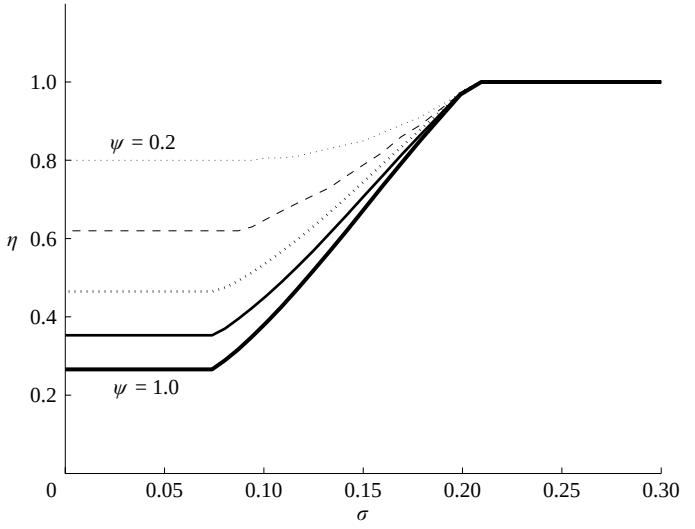


FIGURE 16. $\eta(\sigma, \psi)$ corrected for the drawing together of the plumes, plotted for values of $\psi = 1.0$, 0.8, 0.6, 0.4 and 0.2. The lowest line is for $\psi = 1.0$ and the highest is for $\psi = 0.2$.

This is only a first-order correction, used to establish a scale for the deflection of the plumes. From the minimum value of $\sigma$ for which no interaction occurs, we get $\sigma_u = 0.187$ uncorrected and $\sigma_c = 0.209$ as the corrected value (that is, if $\sigma_0 = 0.209$ then $\bar{\sigma} = 0.187$). This is a 10 % increase in the aspect ratio over which we can expect interaction between the plumes. Further, the choice of the initial length scale for calculating the angle of interaction was fairly arbitrary. However, this value is close to the experimentally evaluated value of $\sigma_c \approx 0.25$. The more significant result of the correction is that, for aspect ratios less than $\sigma_0 = 0.08$, we expect more mixing than the uncorrected calculation (figure 12) suggests.

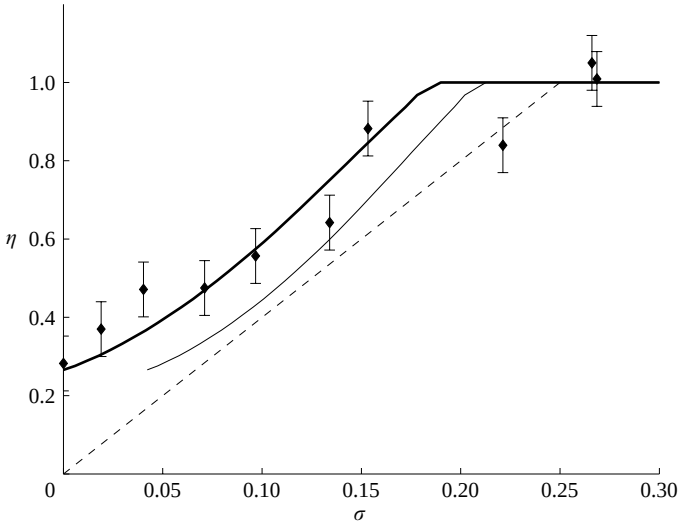


FIGURE 17. Plot of $\eta$ as a function of $\sigma$ for $\psi = 1.0$. The thick line is the uncorrected model prediction from figure 11. The thin line is the prediction corrected for the drawing together of the plumes (figure 14). The dashed line is given by $\eta = \min(4\psi\sigma + 1 - \psi, 1)$.

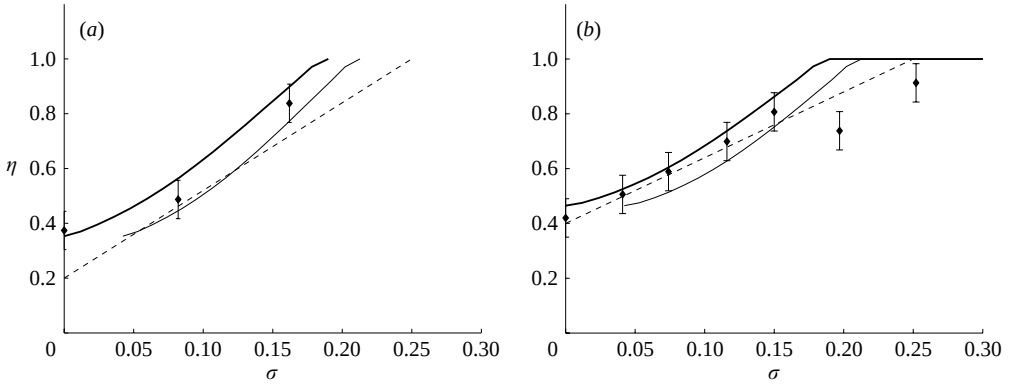


FIGURE 18. Plot of $\eta$ as a function of $\sigma$ for (*a*) $\psi = 0.8$, (*b*) $\psi = 0.6$. The theoretical lines are the same as figure 17.

### 3.10. *Comparison with experimental results*

We now compare the results of our model with the earlier experiments. These are shown in figures 17–20. We recall the two major discrepancies between the linear approximation and the experimental results. First, for equal axially aligned plumes each plume retains some of its buoyancy flux after the collision, that is $\eta(\sigma = 0, \psi < 0.6) > \eta_{\min}$. This feature is clearly captured in figure 17. Second, for $\psi > 0.6$, the rate of increase of $\eta$ with $\sigma$ is less than the linear interpolation. This feature is also captured by the model (see figure 19) which predicts only a slight increase in $\eta$ with separation.

Figures 17–20 show the experimental points from figures 5(*a*)–5(*e*) with the model predictions of figures 12 and 13. The linear approximation shown in figures 5(*a*)–5(*e*) is also included in these figures. There is reasonable agreement between the full model predictions and the experimental results, and the model provides a significantly better

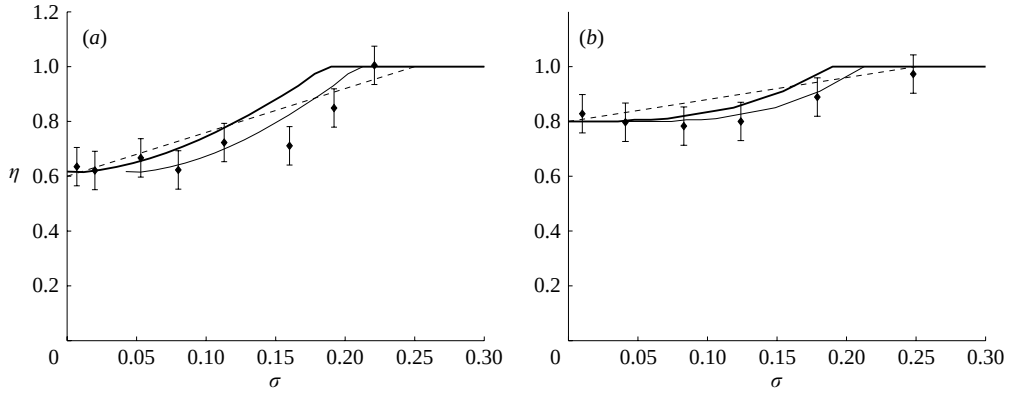


FIGURE 19. Plot of $\eta$ as a function of $\sigma$ for (*a*) $\psi = 0.4$, (*b*) $\psi = 0.2$. The theoretical lines are the same as figure 17.

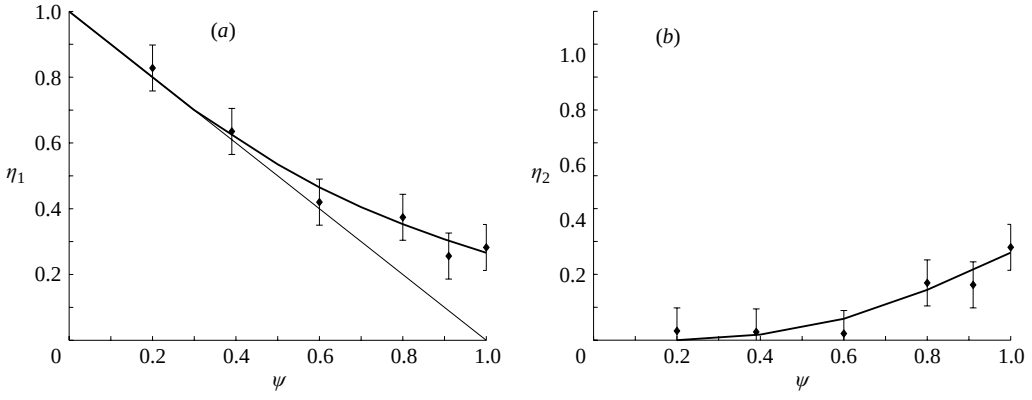


FIGURE 20. (a) Plot of (*a*) $\eta_1$ and (*b*) $\eta_2$ as a function of $\psi$. The thin line is the minimum possible value that conserves buoyancy (2.6). The thick line is the model prediction.

description of our measurements than the simple linear interpolation (2.15). There is particularly good agreement between the entrainment model and our experiments for $\sigma = 0$ (figure 20).

## 4. Conclusions

An experimental technique was developed to measure the buoyancy flux of a plume, based on the ventilation model of Linden *et al.* (1990). This technique was used to measure the buoyancy flux loss that occurs when two plumes with buoyancy fluxes of opposite sign collide. Measurements were made over a wide range of horizontal to vertical aspect ratios $\sigma$ and buoyancy flux ratios $\psi$. The experimental results show that two colliding plumes will exchange buoyancy flux as they pass by each other provided that their horizontal to vertical separation ratio is less than $\sigma \approx 0.25$. For smaller horizontal separations the extent of the buoyancy flux exchange increases to a maximum when the plumes are axially aligned. When one plume is significantly stronger than the other, the weaker plume can be completely absorbed by the stronger plume. However, for buoyancy flux ratios greater than $\psi \approx 0.6$, both plumes emerge

| Parameter | Typical value($x$) | Typical error ($\Delta x/x$) |
|---|---|---|
| $\rho_{\text{source}}$ | 1.1 g cm$^{-3}$ | $10^{-5}$ |
| $\rho_{\text{ambient}}$ | 1.05 g cm$^{-3}$ | $10^{-5}$ |
| $\rho_{\text{layer}}$-$\rho_{\text{ambient}}$ | $2\times10^{-3}$ g cm$^{-3}$ | $5\times10^{-3}$ |
| $g_0'$ | 2 cm s$^{-2}$ | $5\times10^{-3}$ |
| $g'_{\text{source}}$ | 50 cm s$^{-2}$ | $10^{-5}$ |
| $h$ | 1.0 cm | $5\times10^{-2}$ |
| $Q_{\text{source}}$ | 1.0 cm$^{-3}$ s$^{-1}$ | 0.02 |
| $C_d$ | 0.63 | 0.02 |
| $\chi_0$ | 0–3 cm | 0.08 cm |
| $H$ | 10 cm | 0.02 |

TABLE 1. Typical measurements and relative errors for buoyancy flux measurements. Note that the error on the axial separation is an absolute error.

from the collision region with some of their initial buoyancy flux. For axially aligned plumes of equal buoyancy flux ($\psi=1$) each plume retains about a quarter of its original buoyancy flux.

Based on these experimental results a model has been developed to describe the buoyancy flux loss in each plume due to plume–plume collision. The plume conservation equations (Morton *et al.* 1956) were modified to account for the interactions that occur during collision. Two models were considered to describe the exchange of buoyancy flux. Model (A) assumed a bidirectional buoyancy exchange while model (B) a unidirectional exchange. Based on our experimental results we concluded that the unidirectional entrainment model better describes our results. The model was used to predict the total loss in buoyancy flux of the two plumes in terms of their source strengths and separation. A first-order correction to this theory was made to account for the drawing together of the two plumes due to the entrainment field. This first-order model shows significantly better agreement with the experimental results than a simple linear interpolation that assumes complete mixing for $\sigma=0$ and no mixing for $\sigma>0.25$.

N. B. K. would like to thank the British Council and the Association of Commonwealth Universities for their financial support for this research, and we thank Dr S. B. Dalziel for his assistance with the experiments.

## Appendix. Error estimate for experiments

Here we review the possible sources of error in our experiments. In order to establish a value of $\eta$ for any given experiment the following measurements need to be made: $g_0'$, $h$, $F_1$, $A_0$ and $C_d$. It is also necessary to measure the vertical and axial separation, and the buoyancy flux ratio. A summary of typical values and relative errors for these measurements is presented in table 1.

Analysing the impact of the errors listed in table 1 on (2.12), we find

$$\Delta\eta \approx \frac{\partial\eta}{\partial A_0}\Delta A_0 + \frac{\partial\eta}{\partial C_d}\Delta C_d + \frac{\partial\eta}{\partial g_0'}\Delta g_0' + \frac{\partial\eta}{\partial h}\Delta h + \frac{\partial\eta}{\partial F_1}\Delta F_1. \tag{A 1}$$

Dividing both sides by $\eta$ we obtain

$$\frac{\Delta\eta}{\eta} \approx \left|\frac{\Delta A_0}{A_0}\right| + \left|\frac{\Delta C_d}{C_d}\right| + \frac{3}{2}\left|\frac{\Delta g_0'}{g_0'}\right| + \frac{1}{2}\left|\frac{\Delta h}{h}\right| + \left|\frac{\Delta F_1}{F_1}\right|. \tag{A 2}$$

Substituting the values from table 1 gives

$$\frac{\Delta\eta}{\eta} \approx 10^{-4} + 0.02 + \tfrac{3}{2} \times 10^{-5} + \tfrac{1}{2} \times 5 \times 10^{-2} + 0.02 \approx 0.07. \tag{A 3}$$

Errors in evaluating the variables $\psi$ and $\sigma$ are given by

$$\frac{\Delta\psi}{\psi} \approx \left|\frac{\Delta F_1}{F_1}\right| + \left|\frac{\Delta F_2}{F_2}\right| \approx 0.04 \tag{A 4}$$

and

$$\frac{\Delta\sigma}{\sigma} \approx \left|\frac{\Delta\chi_0}{h}\right| \approx 0.01. \tag{A 5}$$

These errors are used to evaluate the error bars for the experimental results plotted.

## REFERENCES


Baines, W. D. 1983 A technique for the measurement of volume flux in a plume. *J. Fluid Mech.* **132**, 247–256.

Baines, W. D. & Turner, J. S. 1969 Turbulent buoyant convection from a source in a confined region. *J. Fluid Mech.* **37**, 51–80.

Bloomfield, L. J. & Kerr, R. C. 2000 A theoretical model of a turbulent fountain. *J. Fluid Mech.* **424**, 197–216.

Cooper, P. & Linden, P. F. 1996 Natural ventilation of an enclosure containing two buoyancy sources. *J. Fluid Mech.* **311**, 153–176.

Gaskin, S. J., Papps, D. A. & Wood, I. R. 1995 The axisymmetric equations for a buoyant jet in a cross flow. *Twelfth Australasian Fluid Mechanics Conference* (ed. R. W. Bilger), pp. 347–350. The University of Sydney.

Hacker, J., Linden, P. F. & Dalziel, S. B. 1996 Mixing in lock release gravity currents. *Dyn. Atmos. Oceans* **24**, 183–195.

Hunt, G. R. & Kaye, N. G. 2001 Virtual origin correction for lazy turbulent plumes. *J. Fluid Mech.* **435**, 377–396.

Kaye, N. B. & Linden P. F. 2004 Coalescing axisymmetric turbulent plumes. *J. Fluid Mech.* **502**, 41–63.

Konig, O. & Fiedler, H. E. 1991 The structure of round turbulent jets in counter-flow: A flow visualisation study. *Advances in Turbulence* (ed. A. V. Johansson & P. H. Alfredsson), pp. 61–66. Springer.

Linden, P. F., Lane-Serff, G. F. & Smeed, D. A. 1990 Emptying filling boxes, the fluid mechanics of natural ventilation. *J. Fluid Mech.* **212**, 309–315.

Massey, B. F. 1989 *Mechanics of Fluids*, 6th Edn. Chapman and Hall.

Morton, B. R., Taylor, G. I. & Turner, J. S. 1956 Turbulent gravitational convection from maintained and instantaneous sources. *Proc. R. Soc. Lond.* A **234**, 1–23.

Moses, E., Zocchi, A. & Libchaber, A. 1993 An experimental study of laminar plumes. *J. Fluid Mech.* **251**, 581–601.

Rouse, H., Yih, C. S. & Humphreys, H. W. 1952 Gravitational convection from a boundary source. *Tellus* **4**, 201–210.

Turner, J. S. 1966 Jets and plumes with negative and reversing buoyancy. *J. Fluid Mech.* **26**, 779–792.

Witze, P. O. & Dwyer, H. A. 1976 The turbulent radial jet. *J. Fluid Mech.* **75**, 401–417.

Yoda, M. & Fiedler, H. E. 1996 The round jet in a uniform counter-flow: Flow visualisation and mean concentration measurements. *Exps. Fluids* **21**, 427–436.